ARTICLES SCIENCE CHINA Materials

mater.scichina.com link.springer.com

Published online 2 June 2017 | doi: 10.1007/s40843-017-9056-1
Sci China Mater 2017, 60(6): 554–562

SPECIAL ISSUE: Biomaterial Foundations of Therapeutic Delivery

Albumin nanoreactor-templated synthesis of Gd_2O_3/CuS hybrid nanodots for cancer theranostics

Ru Wen[1†], Xiaoyan Lv[2†], Tao Yang[2], Yu Li[1], Yong'an Tang[3], Xin Bai[2], Hengte Ke[2*], Junkang Shen[1*] and Huabing Chen[2,3*]

ABSTRACT It remains a great challenge to explore the facile way to fabricate multi-component nanoparticles in theranostic nanomedicine. Herein, an albumin nanoreactor templated synthesis of theranostic Gd_2O_3/CuS hybrid nanodots (NDs) has been developed for multimodal imaging guided photothermal tumor ablation. Gd_2O_3/CuS NDs are found to possess particle size of 4.4 ± 1.1 nm, enhanced longitudinal relaxivity, effective photothermal conversion of 45.5%, as well as remarkable near-infrared fluorescence (NIRF) from Cy7.5-conjugated on albumin corona. The Gd_2O_3/CuS NDs further exhibited good photostability, enhanced cellular uptake, and preferable tumor accumulation. Thus, the Gd_2O_3/CuS NDs generate remarkable NIRF imaging and T_1-weighted magnetic resonance (MR) imaging, and simultaneously result in effective photothermal tumor ablation upon irradiation. The albumin nanoreactor provides a facile and general strategy to synthesize multifunctional nanoparticles for cancer theranostics.

Keywords: albumin nanoreactor, nanodot, theranostics, photothermal therapy, magnetic resonance imaging

INTRODUCTION

Nanomedicine provides extraordinary capabilities for cancer diagnostics and therapeutics [1–5]. The integration of diagnostic imaging and therapy has led to the emergence of theranostic nanoparticles for personalized nanomedicine [6–14]. A variety of theranostic nanoparticles have been recently developed to provide multifunctional properties for achieving effective cancer imaging and simultaneous therapy through the combination of diagnostic and therapeutic components *via* co-loading or chemical conjugation [15–17]. Generally, these nanoparticles frequently suffer from several concerns such as complex compositions and construction, pharmacokinetic inconsistence between imaging and therapeutic agents, as well as the use of clinically unaccepted ingredients. Consequently, it is still a major challenge to develop a facile and rational approach to synthesize high-performance nanoparticles for efficient cancer theranostics.

Recently, some proteins such as albumin, ferritin and aminopeptidase have been extensively explored as biocompatible protein nanoreactors that facilitate the synthesis of metal or metal chalcogenide nanoparticles such as CuS and Ag_2S nanodots (NDs) within their intrinsic cavities through the isotropic or anisotropic growth of nanocrystals [18–21]. The protein nanoreactors possess a satisfactory capacity to achieve a facile construction of ultrasmall nanocrystals with well-defined nanostructures in a mild condition [22]. However, a few efforts have been made to generate multi-component nanoparticles through simultaneous multiple reactions within protein nanoreactor for cancer theranostics. Herein, we developed a facile approach to synthesize Gd_2O_3/CuS hybrid NDs through two precipitation reactions within albumin nanoreactor, leading to multimodal imaging-guided photothermal tumor ablation (Fig. 1).

EXPERIMENTAL SECTION

Preparation of nanodots

Typically, 2.0 mL of 20.0 mmol L^{-1} copper(II) acetate

[1] Department of Radiology, Second Affiliated Hospital of Soochow University, Suzhou 215004, China
[2] Jiangsu Key Laboratory of Translational Research and Therapy for Neuro-Psycho-Diseases, and College of Pharmaceutical Sciences, Soochow University, Suzhou 215123, China
[3] National Engineering Research Center for Nanomedicine, and College of Life Science and Technology, Huazhong University of Science and Technology, Wuhan 430074, China
† These authors contributed equally to this work.
* Corresponding authors (emails: htke@suda.edu.cn (Ke H); shenjunkang@suda.edu.cn (Shen J); chenhb@suda.edu.cn (Chen H))

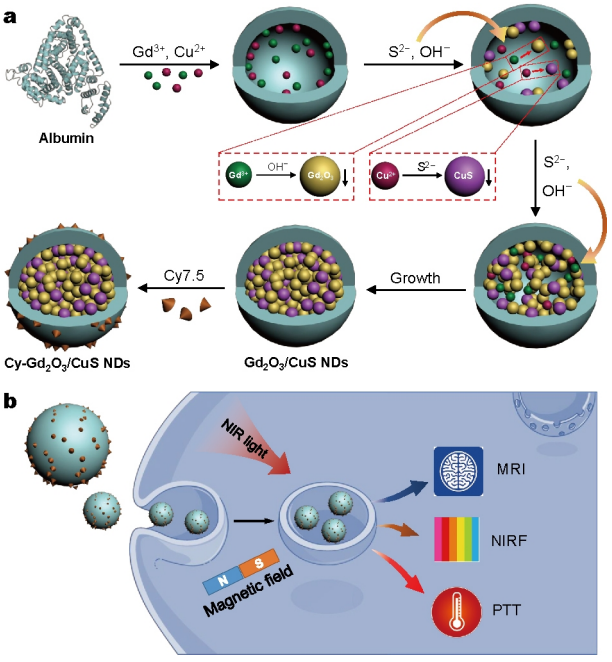

Figure 1 Schematic illustration of (a) albumin nanoreactor-templated construction of Gd_2O_3/CuS NDs and (b) their use for cancer theranostics.

$(Cu(AC)_2)$ and 2.0 mL of 20.0 mmol L^{-1} gadolinium(III) chloride ($GdCl_3$) were added into 10.0 mL of 50.0 mg mL^{-1} bovine serum albumin (BSA) under vigorous stirring. Next, NaOH was used to adjust the pH of the solution to 12. Then, 0.8 mL of 100 mmol L^{-1} Na_2S was added into the mixture. The mixture was further stirred at 55°C for another 4 h, followed by the formation of Gd_2O_3/CuS NDs. The obtained suspension was centrifuged through the ultrafiltration (100 kDa, Millipore) and purified through the dialysis against distilled water for 24 h. To conjugate Cy7.5 with Gd_2O_3/CuS NDs, 1.0 mL of Cy7.5-NHS (0.5 mg mL^{-1}) was mixed with 4.0 mL suspension under stirring in dark overnight to allow the amide reaction between activated carboxyl of Cy7.5 and amine of albumin, followed by the dialysis against distilled water to obtain Cy7.5 conjugated NDs. Different Gd/Cu feed molar ratios at 0.05:1, 0.1:1, 0.25:1, 0.5:1, 1:1 and 2:1 were used in the preparation procedures to obtain hybrid NDs of varied Gd/Cu ratios.

Characterization

Transmission electron microscopy (TEM, Hitachi H-600) was used to observe the morphology of the nanoparticles. The hydrodynamic diameter was measured using dynamic light scattering (DLS, Zetasizer NanoZS90). The absorption spectra of Gd_2O_3/CuS NDs were measured using a UV-vis spectrophotometer (Shimadzu UV2600). Inductively coupled plasma optical emission spectrometer (ICP-OES, VARIAN 710-ES) was applied to quantify the concentrations of Cu and Gd.

Photothermal effect

All light irradiation was conducted using a laser at 785 nm (1.5 W cm^{-2}). To study the photothermal effects of Gd_2O_3/CuS NDs, 0.5 mL Gd_2O_3/CuS NDs at various Cu concentrations ranging from 0.1 to 2.0 mmol L^{-1} were irradiated for 5 min. The temperature of the solutions was monitored using a digital temperature sensor at an interval of 30 s. The temperature elevation (ΔT) was used to evaluate the photothermal effects. To evaluate the photothermal conversion efficiency, Gd_2O_3/CuS NDs at the concentration of 2.0 mmol L^{-1} Cu were irradiated for 12 min, and then the laser was removed for cooling the sample to room temperature. During this process, the temperature of the solution was recorded using a thermometer at an interval of 30 s. To evaluate the photostability, the absorbance at 785 nm was measured under irradiation for different time. To evaluate the ability to maintain the temperature elevations, 0.5 mL Gd_2O_3/CuS NDs at the concentration of 0.5 mmol L^{-1} Cu are subjected to 5 min irradiation (light ON), and then was cooled to room temperature in the absence of irradiation (light OFF), followed by another 4 light ON/OFF cycles.

Cellular uptake

Gd_2O_3/CuS NDs at the concentration of 0.1 mmol L^{-1} Cu were incubated with 4T1 tumor cells (1.0×10^5 cells per well) for 6 h and 24 h, respectively. Then, the cells were treated with trypsin for 3 min at 37°C, followed by cell counting. Afterwards, the cells were digested by nitric acid, and the concentrations of Cu and Gd were measured using ICP-OES, respectively.

Cytotoxicity

The cytotoxicity of Gd_2O_3/CuS NDs under irradiation or not was investigated using MTT assay. 100 μL Gd_2O_3/CuS NDs at various concentrations were incubated with 4T1 tumor cells (5000 cells per well) for 24 h. Then, the cells were rinsed and supplied with 100 μL fresh media, followed by 1.5 W cm^{-2} irradiation at 785 nm for 3 min or not. After another 24 h incubation, the cell viability was evaluated using MTT assay.

Near-infrared fluorescence (NIRF) imaging

All animal operations were in accordance with the institutional animal use and care regulations, College

Reviewer Committees of Soochow University for Animal Use and Welfare. Cy7.5-labelled Gd_2O_3/CuS NDs (Cy7.5-Gd_2O_3/CuS NDs) were intravenously injected into the 4T1 tumor-bearing nude mice at the dose of 75.0 μmol kg^{-1} (n=3) Cu. Then, the *in vivo* fluorescence imaging was performed at 0, 1, 2, 4, 6, 24, 48, and 168 h post-injection using IVIS Lumina II imaging system, respectively. Finally, the average fluorescent intensity at tumor region was calculated.

Magnetic resonance (MR) imaging

For *in vivo* MR imaging, Gd_2O_3/CuS NDs (75.0 μmol kg^{-1} Gd) were intravenously injected into the 4T1 tumor-bearing BALB/c mice. Then, T_1-weight images were obtained at different time using a 1.5 T MR imaging system (Philips, Achieva) with a fat-saturated 3D gradient echo imaging sequence (TR/TE = 400/10 ms, 256×256 matrices, slices = 3, thickness = 2 mm, averages = 4, FOV = 60×60).

Photothermal antitumor efficacy

Gd_2O_3/CuS NDs at the doses of 25.0, 50.0, and 75.0 μmol kg^{-1} Cu were intravenously injected into the tumor-bearing BALB/c mice, respectively. The tumors were exposed to 5 min irradiation at 1.5 W cm^{-2}. Then, the tumor volumes were monitored during subsequent 30 days according to the equation of $V = L \times W^2/2$, where W and L are the tumor measurements at the widest and longest dimensions, respectively. The relative tumor volume was applied to evaluate the antitumor efficacy.

RESULTS AND DISCUSSION

Gd_2O_3/CuS NDs were constructed using albumin as a nanoreactor under a mild condition in water. Gadolinium(III) and copper(II) ions were firstly added to the aqueous solution of BSA for binding with abundant amino acid residues. Then, the pH of the solution was further adjusted to 12, leading to the formation of unfolded BSA with hollow nanocages [23,24]. Afterwards, Gd^{3+} bound with albumin reacted with OH^- to generate Gd_2O_3 nanocrystals, and Na_2S was also added to react with copper ions for generating CuS nanocrystals in the nanoreactor. Thus, the Gd_2O_3/CuS NDs were synthesized in albumin nanoreactor. Cy7.5 was conjugated with amino groups on albumin as an NIRF agent to achieve the fabrication of Cy7.5-Gd_2O_3/CuS NDs (Fig. 1a).

The morphology of the obtained Gd_2O_3/CuS NDs was characterized using TEM, indicating 4.4 ± 1.1 nm in diameter with a uniform distribution (Fig. 2a). DLS measure-

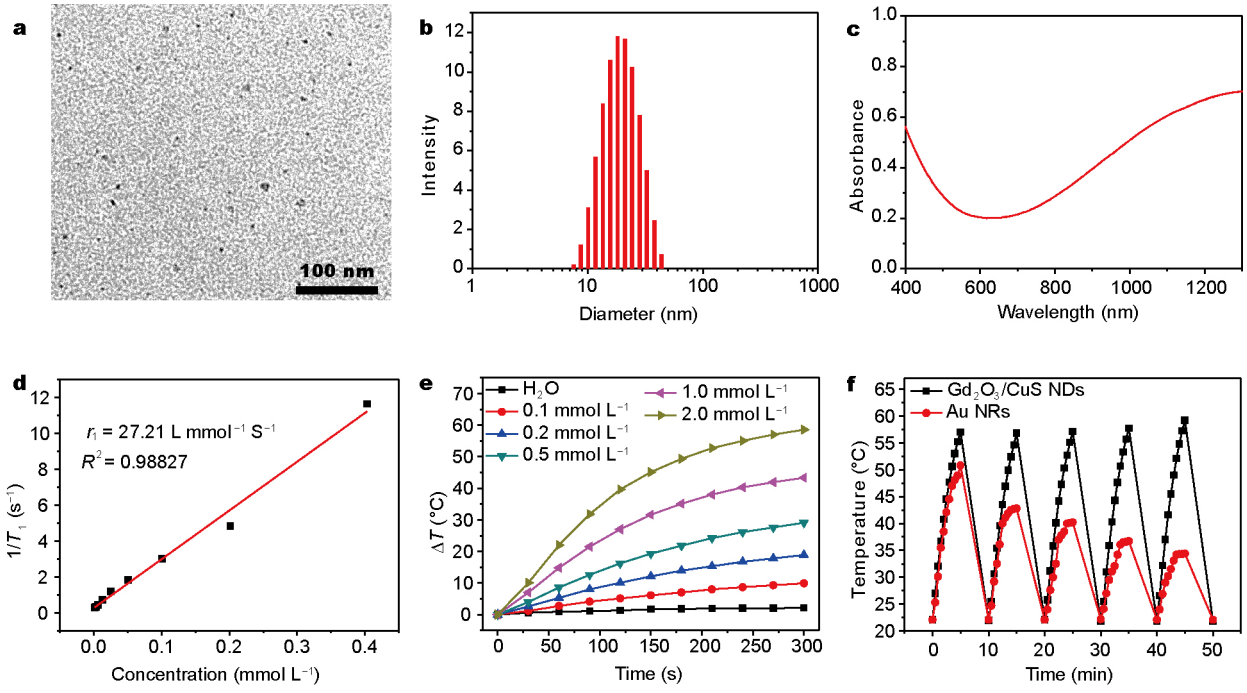

Figure 2 (a) TEM image, (b) size distribution and (c) UV-vis absorbance spectrum of Gd_2O_3/CuS NDs; (d) relaxivity of Gd_2O_3/CuS NDs from T_1-weighted maps in MR phantoms; (e) temperature elevations of Gd_2O_3/CuS NDs in 5 min at various Cu concentrations under 785 nm irradiation (1.5 W cm^{-2}); (f) temperature elevations of Gd_2O_3/CuS NDs and Au NRs under five laser ON/OFF cycles (785 nm,1.5 W cm^{-2}).

ment indicates that the Gd_2O_3/CuS NDs have a hydrodynamic diameter of 18.2 ± 2.2 nm owing to the presence of protein corona, implying a potential passive targeting capability through enhanced permeation and retention (EPR) effect (Fig. 2b). The UV-vis absorption spectrum of the Gd_2O_3/CuS NDs in water displayed a strong and board absorbance in the near infrared (NIR) region from 700 to 1300 nm, possibly resulting from the presence of CuS (Fig. 2c). A thin film of Gd_2O_3/CuS NDs on the glass silde was prepared to avoid the strong absorbance of water, and the absorption spectrum was obtained at the range of 400–2400 nm (Fig. S1). The results suggested the strong localized surface plasmon resonance (LSPR) peak at ~1460 nm from CuS nanocrystals, confirming the NIR light triggered potent photothermal effect. Several small peaks from 1800 to 2400 nm could be attributed to the absorbance of BSA, demonstrating the presence of albumin in the nanocomposites. The X-ray diffraction (XRD) pattern of NDs showed the peaks of [101] and [110] from hexagonal CuS, and peaks of [222] and [400] from cubic Gd_2O_3, confirming the successful fabrication of hybrid NDs of both Gd_2O_3 and CuS nanocrystals (Fig. S2).

Given that Gd_2O_3 is a component with longitudinal relaxivity [25–29], the longitudinal proton relaxation time (T_1) of Gd_2O_3/CuS NDs was measured using T_1-weighted mapping at the magnetic field of 1.5 T for calculating their relaxivities (Fig. S3). The Gd/Cu molar ratios of the resulted Gd_2O_3/CuS NDs were measured to be 0.04:1, 0.06:1, 0.15:1, 0.30:1, 0.60:1 and 1.20:1 at various Gd/Cu feed molar ratios, respectively. Remarkably, Gd/Cu molar ratio had distinct influence on their relaxivity, indicating a gradual decrease from 50.3 to 27.2 $L\,mmol^{-1}\,s^{-1}$ along with the increase of Gd/Cu ratio in the NDs (Fig. 2d and Fig. S4), probably due to geometrical confinement of gadolinium in the restricted space of albumin cavity, which influences the paramagnetic behavior of the Gd^{3+} ions [25,30]. Nevertheless, the Gd_2O_3/CuS NDs exhibited relaxivity of about 9–17-fold as compared to Gd-DTPA (3.2 $L\,mmol^{-1}\,s^{-1}$), indicating a superior relaxivity for potential MRI. To balance the dosing concentration of Gd_2O_3 and CuS, the Gd/Cu molar ratio of 1.20:1 was selected for subsequent studies.

To evaluate the photothermal effect, temperature elevation of the Gd_2O_3/CuS NDs at various Cu concentrations was evaluated under 1.5 W cm^{-2} irradiation at 785 nm (Fig. 2e). The Gd_2O_3/CuS NDs exhibited a fast temperature elevation of 9.9°C at a relatively low concentration of 0.1 mmol L^{-1}, displaying a distinct photothermal effect. Remarkably, the Gd_2O_3/CuS NDs displayed a concentration-dependent temperature elevation, which is highly important for causing potent photo-induced hyperthermia (>45°C) [31]. Subsequently, the Gd_2O_3/CuS NDs were further found to have a photothermal conversion efficiency of ~45.5% (Fig. S5), which is much higher than that of the extensively studied photothermal agents such as Au nanorods (Au NRs, ~ 13%) [32].

The stability of Gd_2O_3/CuS NDs under NIR light irradiation was evaluated using temperature monitoring. The Gd_2O_3/CuS NDs were subjected to 785 nm irradiation at 1.5 W cm^{-2} for 5 min (light ON). Then, the irradiation was removed and the Gd_2O_3/CuS NDs were cooled to room temperature in the absence of irradiation (light OFF). This procedure was further repeated for another four light ON/OFF cycles. The Gd_2O_3/CuS NDs exhibited tremendous temperature increase of 35.0°C after first irradiation, and no significant change of temperature elevation was observed during the subsequent four cycles (Fig. 2f). In contrast, Au NRs displayed a significant temperature decrease after laser ON/OFF cycles, as well as obvious decrease of NIR absorbance compared with the Gd_2O_3/CuS NDs (Fig. S6). Moreover, the Gd_2O_3/CuS NDs also showed no remarkable change in the absorbance at 785 nm under continuous 15 min irradiation, further confirming that these NDs have ideal photostability (Fig. S7). It indicates that the Gd_2O_3/CuS NDs have good photostability to maintain effective light treatment for theranostics.

To evaluate the cellular uptake, the Gd_2O_3/CuS NDs were incubated with 4T1 tumor cells for 6 and 24 h, respectively. The Gd_2O_3/CuS NDs exhibited time-dependent cellular uptakes of Cu and Gd (Fig. 3a and Fig. S8a). Additionally, the endocytic pathway of the Gd_2O_3/CuS NDs was also evaluated using different pathway inhibitors (Fig. 3b and Fig. S8b), indicating that they have a clathrin-mediated endocytic pathway that is also energy-dependent. To investigate the intracellular distribution, the Cy7.5-Gd_2O_3/CuS NDs were incubated with 4T1 cells stained with Lysotracker Green DND-26 and Hoechst 33342 for 2 h, followed by observation using confocal laser scanning microscopy (CLSM). The Cy7.5-Gd_2O_3/CuS NDs in red fluorescence exhibited a co-localization percentage of 98% with the lysosomes in green fluorescence, indicating a preferable distribution into lysosomes through clathrin-mediated endocytosis (Fig. 3c). Afterwards, the photo-induced cytotoxicity of Gd_2O_3/CuS NDs was further carried out against 4T1 tumor cells for 24 h, followed by 3 min irradiation (785 nm, 1.5 W cm^{-2}). the Gd_2O_3/CuS NDs showed negligible cell damage (IC_{50}, 318 μmol L^{-1}) with the absence of irradiation, implying the desirable biocompatibility of Gd_2O_3/CuS NDs in dark. Conversely, the Gd_2O_3/CuS NDs

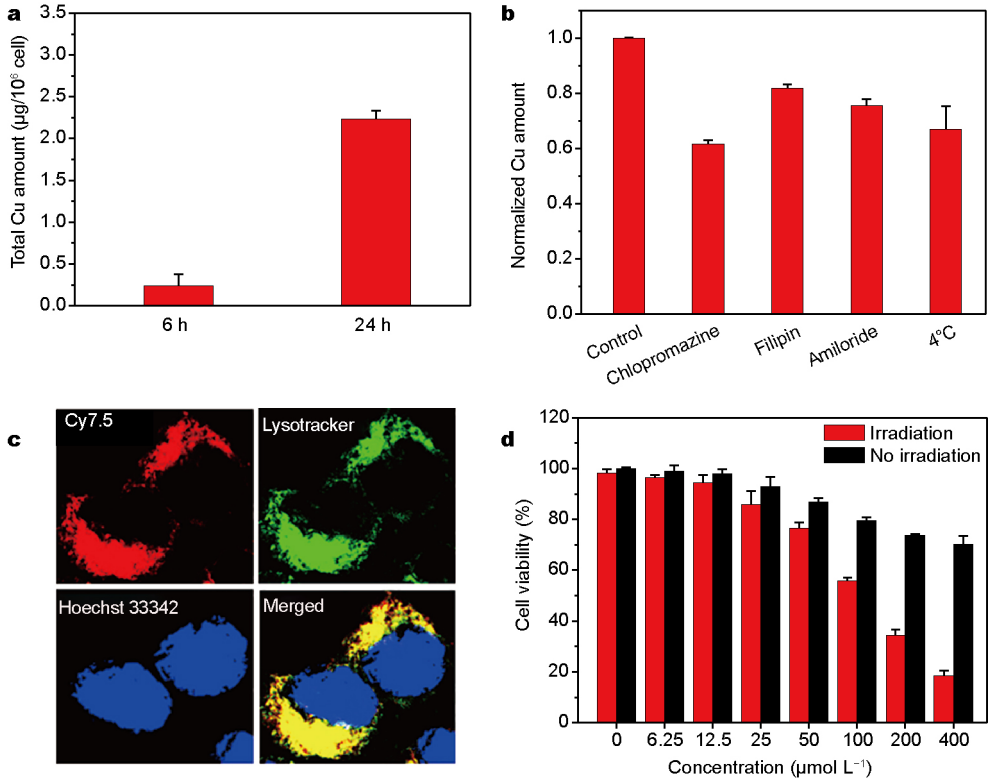

Figure 3 (a) Total amount of Cu internalized by 4T1 cells after 6 and 24 h incubation with Gd_2O_3/CuS NDs, respectively; (b) endocytic pathway of Gd_2O_3/CuS NDs into 4T1 cells; (c) intracellular distribution of Cy7.5-labelled Gd_2O_3/CuS NDs in 4T1 cells stained by Lysotracker and Hoechst 33342; (d) cytotoxicity of Gd_2O_3/CuS NDs upon NIR irradiation or not (785 nm,1.5 W cm^{-2}).

exhibited severe cell injury (IC_{50}, 111 μmol L^{-1}) with concentration-dependent behavior under irradiation (Fig. 3d), probably owing to the concentration-dependent photothermal effects and effective cellular uptake. Remarkably, the Gd_2O_3/CuS NDs exhibit an ideal ability to produce photothermal damage against tumor cells with great potential for *in vivo* photothermal therapy (PTT).

The pharmacokinetic behavior of the Gd_2O_3/CuS NDs was investigated on healthy Balb/c mice by monitoring of Gd concentration in the blood plasma. The results exhibited an elimination half-life time ($t_{1/2\beta}$) of 1.58 h (Fig. S9, Table S1). The biodistribution behavior of the Gd_2O_3/CuS NDs was further evaluated at 24 h post-injection (Fig. S10). Gd_2O_3/CuS NDs exhibited a primary distribution at tumor during 24 h, probably owing to their significant EPR effect. To demonstrate the multimodal imaging capacity of Cy7.5-Gd_2O_3/CuS NDs, the *in vivo* NIRF imaging was carried out on the mice bearing 4T1 tumors. The release profile study of Cy7.5 from the Cy7.5-Gd_2O_3/CuS NDs showed only a slight release during 24 h in the physiological conditions, indicating the preferable stability of conjugated Cy7.5 in the NDs (Fig. S11). Interestingly, the Cy7.5-Gd_2O_3/CuS NDs exhibited obvious NIRF signals at tumor during 7 days (Fig. 4a, b), suggesting that these NDs have an effective NIRF imaging capacity with good sensitivity. In addition, it also shows that the Cy7.5-Gd_2O_3/CuS NDs resulted in a long-time retention of NIRF signals at tumor, implying their good retention behavior at tumor for flexible PTT treatment. Moreover, MR imaging of the Gd_2O_3/CuS NDs was further studied on the mice bearing 4T1 tumor. As shown in Fig. 4c, d, the MR intensity at tumor sites injected with hybrid NDs showed significant enhancement at 2, 12 and 24 h post-injection, while Gd-DTPA as a control had no obvious influence on the MR intensity at tumor sites, suggesting a remarkable contrast-enhanced MRI capacity of Gd_2O_3/CuS NDs to provide an imaging modality with high spatial resolution.

To demonstrate the *in vivo* hyperthermia of Gd_2O_3/CuS NDs, the mice bearing 4T1 tumor were treated with NDs at different doses through a single-dose injection, followed by 5 min irradiation (785 nm, 1.5 W cm^{-2}), and then their infrared thermographs were captured using a thermal imaging camera (Fig. 5a). The calculated temperature profiles show that Gd_2O_3/CuS at the dose of 25.0 μmol kg^{-1} Cu

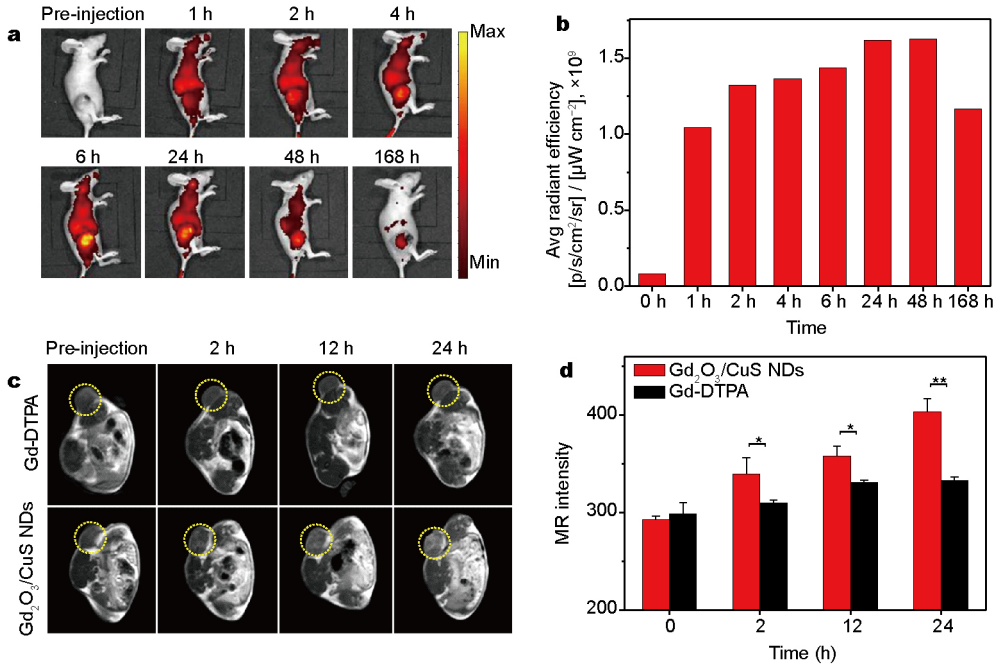

Figure 4 (a) *In vivo* NIRF imaging and (b) calculated intensity of the mice injected with Cy7.5-Gd_2O_3/CuS NDs during 168 h post-injection; (c) *in vivo* MR imaging and (d) calculated MR intensity of the tumor areas (highlighted in yellow circles) from the mice injected with Gd_2O_3/CuS NDs and Gd-DTPA at 0, 2, 12 and 24 h post-injection, respectively (*p<0.05, **p<0.01).

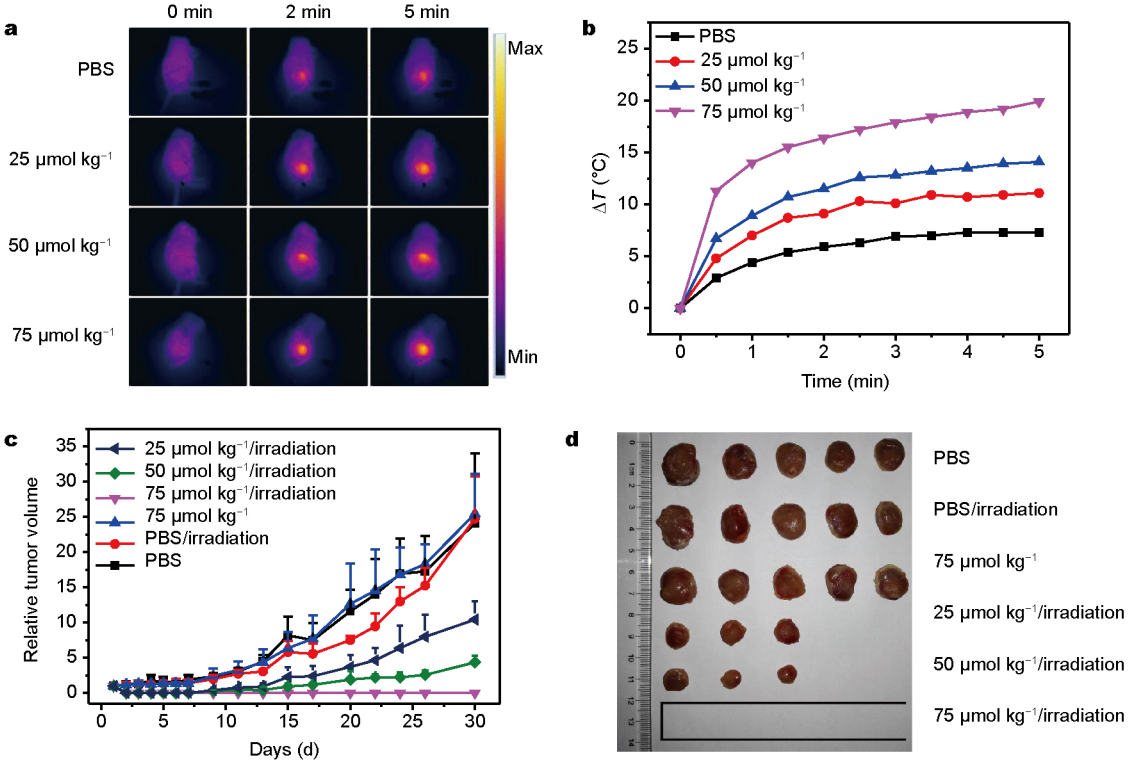

Figure 5 (a) Infrared thermography and (b) corresponding temperature elevation at tumor region of the mice injected with Gd_2O_3/CuS NDs at various doses under 1.5 W cm^{-2} irradiation (785 nm,5 min); (c) tumor growth profiles of the mice treated with Gd_2O_3/CuS NDs at different doses under 785 nm irradiation or not, (d) photographs of the tumors extracted from the mice at the end of experiment.

resulted in the temperature elevation of 11.1°C at the tumor under irradiation (Fig. 5b), suggesting a remarkable hyperthermia even at a relatively low dosage. Importantly, higher temperature elevations of 14.1°C and 19.9°C at the tumors were achieved at the doses of 50.0 and 75.0 μmol kg^{-1} Cu under irradiation, respectively, suggesting a dose-dependent hyperthermia. Possibly, both high photothermal conversion efficiency and enhanced tumor accumulation contribute to superior hyperthermia at tumor, which is able to facilitate *in vivo* PTT treatment.

The *in vivo* photothermal anticancer efficacy of the Gd_2O_3/CuS NDs was evaluated using 4T1 tumor-bearing mice at various doses through a single-dose intravenous administration, followed by 785 nm irradiation for 5 min (Fig. 5c, d). Phosphate buffered saline (PBS) caused ~23-fold increase of tumor volume as compared to their original volumes with or without irradiation, confirming that the growth of tumor is not significantly affected by the light irradiation itself. A similar tumor growth behavior was observed for the Gd_2O_3/CuS NDs at the highest dose of 75.0 μmol kg^{-1} without irradiation, indicating that they had no influence on the tumor growth in the absence of irradiation. Interestingly, the Gd_2O_3/CuS NDs at the doses of 25.0 and 50.0 μmol kg^{-1} Cu resulted in rapid tumor ablation upon irradiation, but displayed remarkable tumor regrowth after ~10 day post-irradiation. Most importantly, the Gd_2O_3/CuS NDs at 75 μmol kg^{-1} Cu exhibited complete tumor ablation without any regrowth, implying that the tumor temperature elevation of ~19.9°C effectively results in the total tumor ablation without any regrowth. Distinctly, the good photostability, high photothermal conversion efficiency, and preferable tumor accumulation of Gd_2O_3/CuS NDs synergistically contribute to the desirable anticancer efficacy.

Hematoxylin & eosin (H&E) staining of tumor sections from mice with various treatments was carried out to validate the photothermal damage (Fig. S12). Severe hemorrhagic inflammation and destructive cell necrosis could be found at the tumor of mice treated with Gd_2O_3/CuS NDs at 6 h post-irradiation. In contrast, PBS and Gd_2O_3/CuS NDs without irradiation exhibited no remarkable cell damage. Additionally, no noticeable influence on major tissues such as heart, liver, spleen, lung and kidney was observed (Fig. S12).

CONCLUSIONS

In summary, we demonstrated a facile synthesis of Gd_2O_3/CuS hybrid NDs through the albumin nanoreactor for NIRF/MR imaging and simultaneous photothermal tumor ablation. The Gd/Cu ratios can be tuned in the NDs for favorable longitudinal relaxivity, resulting in significant enhanced MR imaging with spatial resolution. The Gd_2O_3/CuS NDs can be easily conjugated with Cy7.5 for further NIRF imaging with good sensitivity, facilitating their complementary NIRF/MR imaging. The Gd_2O_3/CuS NDs also possessed good photostability, high photothermal conversion efficiency, as well as enhanced cellular uptake and tumor accumulation, thereby facilitating precise tumor ablation upon irradiation. Our albumin nanoreactor boosts a facile and universal approach to develop versatile nanomaterials for cancer theranostics.

Received 15 April 2017; accepted 25 May 2017; published online 2 June 2017

1 Ferrari M. Cancer nanotechnology: opportunities and challenges. Nat Rev Cancer, 2005, 5: 161–171
2 Wang X, Yang L, Chen ZG, *et al.* Application of nanotechnology in cancer therapy and imaging. CA-A Cancer J Clinicians, 2008, 58: 97–110
3 Nie S, Xing Y, Kim GJ, *et al.* Nanotechnology applications in cancer. Annu Rev Biomed Eng, 2007, 9: 257–288
4 Farokhzad OC, Langer R. Nanomedicine: Developing smarter therapeutic and diagnostic modalities. Adv Drug Deliver Rev, 2006, 58: 1456–1459
5 Barreto JA, O'Malley W, Kubeil M, *et al.* Nanomaterials: applications in cancer imaging and therapy. Adv Mater, 2011, 23: H18–H40
6 Warner S. Diagnostics plus therapy = theranostics. Scientist, 2004, 18: 38–39
7 Mura S, Couvreur P. Nanotheranostics for personalized medicine. Adv Drug Deliver Rev, 2012, 64: 1394–1416
8 Chen X, Gambhir SS, Cheon J. Theranostic nanomedicine. Acc Chem Res, 2011, 44: 841–841
9 Cheng L, Liu J, Gu X, *et al.* PEGylated WS_2 Nanosheets as a multifunctional theranostic agent for *in vivo* dual-modal CT/photoacoustic imaging guided photothermal therapy. Adv Mater, 2014, 26: 1886–1893
10 Liu T, Shi S, Liang C, *et al.* Iron oxide decorated MoS_2 nanosheets with double PEGylation for chelator-free radiolabeling and multimodal imaging guided photothermal therapy. ACS Nano, 2015, 9: 950–960
11 Sumer B, Gao J. Theranostic nanomedicine for cancer. Nanomedicine, 2008, 3: 137–140
12 Melancon MP, Zhou M, Li C. Cancer theranostics with near-infrared light-activatable multimodal nanoparticles. Acc Chem Res, 2011, 44: 947–956
13 Li Y, Bai X, Xu M, *et al.* Photothermo-responsive Cu_7S_4@polymer nanocarriers with small sizes and high efficiency for controlled chemo/photothermo therapy. Sci China Mater, 2016, 59: 254–264
14 Mathiyazhakan M, Upputuri PK, Sivasubramanian K, *et al. In situ* synthesis of gold nanostars within liposomes for controlled drug release and photoacoustic imaging. Sci China Mater, 2016, 59: 892–900
15 Tang Y, Hu J, Elmenoufy AH, *et al.* Highly efficient FRET system capable of deep photodynamic therapy established on X-ray excited mesoporous LaF_3:Tb scintillating nanoparticles. ACS Appl Mater Interfaces, 2015, 7: 12261–12269

16 Elmenoufy AH, Tang Y, Hu J, *et al.* A novel deep photodynamic therapy modality combined with CT imaging established *via* X-ray stimulated silica-modified lanthanide scintillating nanoparticles. Chem Commun, 2015, 51: 12247–12250
17 Mou J, Chen Y, Ma M, *et al.* Facile synthesis of liposome/$Cu_{2-x}S$-based nanocomposite for multimodal imaging and photothermal therapy. Sci China Mater, 2015, 58: 294–301
18 Wang Y, Yang T, Ke H, *et al.* Smart albumin-biomineralized nanocomposites for multimodal imaging and photothermal tumor ablation. Adv Mater, 2015, 27: 3874–3882
19 Wang Z, Huang P, Jacobson O, *et al.* Biomineralization-inspired synthesis of copper sulfide–ferritin nanocages as cancer theranostics. ACS Nano, 2016, 10: 3453–3460
20 Xie J, Zheng Y, Ying JY. Protein-directed synthesis of highly fluorescent gold nanoclusters. J Am Chem Soc, 2009, 131: 888–889
21 Sun C, Yang H, Yuan Y, *et al.* Controlling assembly of paired gold clusters within apoferritin nanoreactor for *in vivo* kidney targeting and biomedical imaging. J Am Chem Soc, 2011, 133: 8617–8624
22 Yang T, Wang Y, Ke H, *et al.* Protein-nanoreactor-assisted synthesis of semiconductor nanocrystals for efficient cancer theranostics. Adv Mater, 2016, 28: 5923–5930
23 Tanford C, Buzzell JG, Rands DG, *et al.* The reversible expansion of bovine serum albumin in acid solutions. J Am Chem Soc, 1955, 77: 6421–6428
24 Bro P, Singer SJ, Sturtevant JM. On the aggregation of bovine serum albumin in acid solutions. J Am Chem Soc, 1958, 80: 389–393
25 Bridot JL, Faure AC, Laurent S, *et al.* Hybrid gadolinium oxide nanoparticles: multimodal contrast agents for *in vivo* imaging. J Am Chem Soc, 2007, 129: 5076–5084
26 Park JY, Baek MJ, Choi ES, *et al.* Paramagnetic ultrasmall gadolinium oxide nanoparticles as advanced T_1 MRI contrast agent: account for large longitudinal relaxivity, optimal particle diameter, and *in vivo* T_1 MR images. ACS Nano, 2009, 3: 3663–3669
27 Li F, Zhi D, Luo Y, *et al.* Core/shell Fe_3O_4/Gd_2O_3 nanocubes as T_1–T_2 dual modal MRI contrast agents. Nanoscale, 2016, 8: 12826–12833
28 Eurov DA, Kurdyukov DA, Kirilenko DA, *et al.* Core–shell monodisperse spherical mSiO$_2$/Gd_2O_3:Eu^{3+}@mSiO$_2$ particles as potential multifunctional theranostic agents. J Nanopart Res, 2015, 17: 82
29 Xu Z, Gao Y, Huang S, *et al.* A luminescent and mesoporous core-shell structured Gd_2O_3:Eu^{3+}@nSiO$_2$@mSiO$_2$ nanocomposite as a drug carrier. Dalton Trans, 2011, 40: 4846
30 Ananta JS, Godin B, Sethi R, *et al.* Geometrical confinement of gadolinium-based contrast agents in nanoporous particles enhances T_1 contrast. Nat Nanotech, 2010, 5: 815–821
31 Chu KF, Dupuy DE. Thermal ablation of tumours: biological mechanisms and advances in therapy. Nat Rev Cancer, 2014, 14: 199–208
32 Hessel CM, Pattani VP, Rasch M, *et al.* Copper selenide nanocrystals for photothermal therapy. Nano Lett, 2011, 11: 2560–2566

Acknowledgments This work was financially supported by the National Natural Science Foundation of China (31422021, 51473109, and 81501585), National Basic Research Program of China (2014CB931900), Natural Science Foundation of Jiangsu Province of China (BK20150348), Natural Science Foundation of the Jiangsu Higher Education Institutions of China (15KJB310019), China Postdoctoral Science Foundation (2015M570475 and 2016T90496), Priority Academic Program Development of Jiangsu Higher Education Institutions (PAPD), Jiangsu Key Laboratory of Translational Research and Therapy for Neuro-Psycho-Diseases, Open Fund of CAS Key Laboratory of Nano-Bio Interface (16NBI02), and Jiangsu Undergraduates Innovation and Entrepreneurship Program (20150285075Y).

Author contributions Chen H and Shen J designed the study; Wen R prepared the samples; Wen R, Lv X and Bai X performed the characterizations, cell and animal experiments; Wen R and Li Y carried out the imaging experiments; Ke H and Chen H wrote the paper with support from Yang T and Tang Y. All authors contributed to the general discussion.

Conflict of interest The authors declare that they have no conflict of interest.

Supplementary information Additional experimental details and supporting data are available in the online version of the paper.

Ru Wen is currently a Master candidate at the Department of Radiology, Second Affiliated Hospital of Soochow University. Her research interests include the development and medical application of novel magnetic resonance imaging agents.

Xiaoyan Lv is currently a Master candidate at the College of Pharmaceutical Sciences, Soochow University. Her research interests focus on the development of multifunctional nanoparticles for multimodal cancer imaging and photothermal therapy.

Hengte Ke is currently an assistant professor at the College of Pharmaceutical Sciences, Soochow University. He received his PhD degree of biomedical engineering from Harbin Institute of Technology in 2014, and worked as a visiting scholar at the University of Massachusetts, USA from 2012 to 2013. His research focuses on theranostic nanomedicine and multimodal imaging probes.

Junkang Shen is currently a full professor and chief physician at the Department of Radiology, Second Affiliated Hospital of Soochow University. He received his Master degree of medicine in 1999. His research focuses on clinical magnetic resonance imaging diagnosis.

Huabing Chen is currently a full professor at the College of Pharmaceutical Sciences, Soochow University. He received his PhD degree of biopharmaceutical engineering in 2008 from Huazhong University of Science & Technology. Then he worked as a postdoc at the University of Texas Southwestern Medical Center at Dallas and University of Tokyo from 2008 to 2012. His research interests include biomimetic protein nanoparticles for cancer theranostics and self-assembled nanoparticles for photo-induced cancer therapy.

Gd_2O_3/CuS复合白蛋白纳米粒的合成及其在肿瘤诊疗一体化中的应用

温茹[1†], 吕小燕[2†], 杨涛[2], 李誉[1], 唐永安[3], 柏欣[2], 柯亨特[2*], 沈钧康[1*], 陈华兵[2,3*]

摘要 本文采用白蛋白纳米反应器合成了Gd_2O_3/CuS双组分复合纳米粒, 并将其成功应用于肿瘤的诊断与治疗. 研究发现复合纳米粒中Gd/Cu比例可有效调控其纵向弛豫系数, 其磁共振造影性能数倍于Gd-DTPA. 同时, 可通过化学偶联在蛋白表面修饰近红外荧光探针Cy7.5, 得到Cy7.5-Gd_2O_3/CuS纳米粒, 实现近红外荧光成像与磁共振成像的多模态成像. 该复合纳米粒具有良好的光稳定性、较高的光热转换系数、较强的细胞摄取和肿瘤靶向效应, 实现了精确的肿瘤光热消融治疗. 该方法提供了一种快速、简便、通用的多组分纳米粒构建平台, 为肿瘤诊疗一体化纳米材料的发展提供了新的契机.